Inorganic Chemistry

Article

pubs.acs.org/IC

Emissive Osmium(II) Complexes with Tetradentate Bis(pyridylpyrazolate) Chelates

Shih-Han Chang,[†] Chun-Fu Chang,[†] Jia-Ling Liao,[†] Yun Chi,*[,†] Dong-Ying Zhou,[‡] Liang-Sheng Liao,*[,‡] Tzung-Ying Jiang,[§] Tsao-Pei Chou,[§] Elise Y. Li,*[,§] Gene-Hsiang Lee,[⊥] Ting-Yi Kuo,[⊥] and Pi-Tai Chou[⊥]

[†]Department of Chemistry, National Tsing Hua University, Hsinchu 30013, Taiwan

[‡]Institute of Functional Nano & Soft Materials, SooChow University, Suzhou 215123, China

[§]Department of Chemistry, National Taiwan Normal University, Taipei 11677, Taiwan

[⊥]Department of Chemistry, National Taiwan University, Taipei 10617, Taiwan

Supporting Information

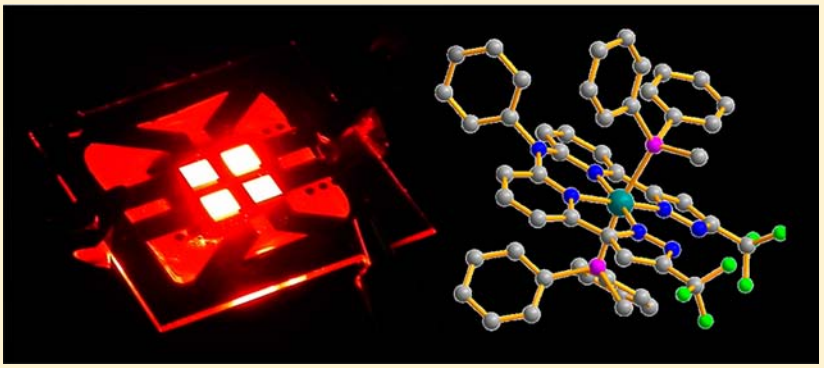

ABSTRACT: A tetradentate bis(pyridylpyrazolate) chelate, **L**, is assembled by connecting two bidentate 3-(trifluoromethyl)-5-(2-pyridyl)pyrazole chelates at the 6 position of the pyridyl fragment with a phenylamido appendage. This chelate was then utilized in the synthesis of three osmium(II) complexes, namely, $[Os(L)(CO)_2]$ (**4**), $[Os(L)(PPh_2Me)_2]$ (**5**), and $[Os(L)(PPhMe_2)_2]$ (**6**). Single-crystal X-ray structural analyses were executed on **4** and **5** to reveal the bonding arrangement of the **L** chelate. Phosphine-substituted derivatives **5** and **6** are highly emissive in both solution and the solid state, and their photophysical properties were measured and discussed on the basis of computational approaches. For application, fabrication and analysis of organic light-emitting diodes (OLEDs) were also carried out. The OLEDs using **5** and **6** as dopants exhibit saturated red emission with maximum external quantum efficiencies of 9.8% and 9.4%, respectively, which are higher than that of the device using $[Ir(piq)_3]$ as a red-emitting reference sample. Moreover, for documentation, **5** and **6** also achieve a maximum brightness of 19540 cd·m^{-2} at 800 mA·cm^{-2} (11.6 V) and 12900 cd·m^{-2} at 500 mA·cm^{-2} (10.5 V), respectively.

INTRODUCTION

Recently, there is a growing interest in the emissive third-row transition-metal complexes because they are crucial for the fabrication of highly efficient organic light-emitting diodes (OLEDs).[1] The strong spin−orbit coupling induced by their central heavy metal atoms, such as osmium(II), iridium(III), and platinum(II), promotes an efficient singlet/triplet intersystem crossing and facilitates strong luminescence in the as-fabricated OLEDs by harvesting both the singlet and triplet excitons. As a result, more emphasis has been put forth on designing such late-transition-metal phosphors, characterizing their photophysical properties, and fabricating practical OLEDs with the newly explored materials.

For the emissive transition-metal chelates, the typical architecture comprises at least one bidentate chelate to serve as the chromophore. Thus, upon variation of the skeletal designs or even the attached substituents, their luminescent properties, particularly the emission peak wavelengths, were able to be fine-tuned, the strategy of which has been supported by a computational approach and experimentally achieved in numerous reports.[2] In studies for osmium(II) complexes, one example is the trisubstituted $[Os(N^\wedge N)_3]^{2+}$ (N^N = 2,2′-bipyridine, phenanthroline, and analogues), which showed emission at λ_{max} = 650−680 nm originating from the triplet metal-to-ligand charge-transfer (MLCT) excited states.[3] Relevant ionic osmium(II) metal complexes have emerged as promising candidates for applications in both OLED and solid-state electroluminescent (EL) devices.[4] In one seminal case, the successful replacement of phenanthroline in $[Os(phen)_3]^{2+}$ with chelating dppe [i.e., 1,2-bis(diphenylphosphino)ethane] gave $[Os(phen)_2(dppe)]^{2+}$ and $[Os(phen)(dppe)_2]^{2+}$, for

Received: December 24, 2012
Published: April 26, 2013

   dx.doi.org/10.1021/ic302829e | *Inorg. Chem.* 2013, 52, 5867−5875

which the electron-accepting phosphine stabilized the metal d_π orbitals and resulted in a substantial blue shift of the emission wavelengths.[5] Recently, relevant examination was switched to the charge-neutral osmium(II) complexes with chelating bipyridine,[6] cyclometalate,[7] or pyridylazolate[8] in attempts to explore their photophysical behaviors and/or as emitters for latent OLED applications. Furthermore, these osmium(II) complexes had showed prominent emission in solution or the solid state, covering the whole visible region and even beyond, i.e., from true-blue,[9] green,[10] red, and even near-IR[11] depending on the design of the chromophoric chelate and ligated ancillary; the latter is mainly for tuning of the oxidation potential of the central Os^{II} atom.

Along this scientific content, amid assembly of the phosphorescent metal complexes, there is also a growing interest of using multidentate chromophores (cf. the traditional bidentate chromophores) for their extended π conjugation and enhanced metal chelate stabilization energy. This maneuver seems to be quite successful for the platinum(II) systems, for which both tridentate and tetradentate chelates are routinely employed in the application of luminescent, chemosensing, and various optoelectronic materials,[12] by taking advantage of their square-planar coordination geometry. In comparison, as to the osmium(II) system, for which the most stable coordination geometry is now changed to an octahedron, studies are more focused on the chelates such as terpyridine[13] and functionalized tridentate analogues,[14] leaving only a handful of documents dealing with the tetradentate chelates such as salen or porphyrin.[15] In contrast to the cyclic geometry of porphyrin, it is expected that the open framework of salen would allow the stepwise formation of metal−ligand bonding around the Os^{II} center, which is essential for gaining insight into the mechanism en route to the designated reaction products.

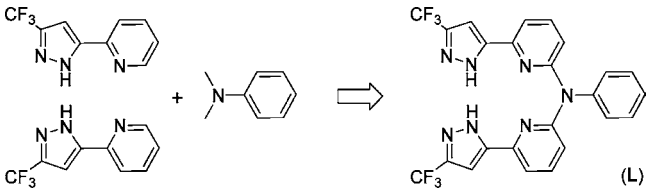

To avoid the inherent constraint imposed by the cyclic arrangement of the tetradentate chelate, we herein describe a new kind of flexible chelate, **L**, which is assembled from two 2-pyridylpyrazole units by linking them with a single phenylamido appendage. We choose this design because it can be easily obtained using procedures similar to those previously published for its bidentate counterpart.[16] Moreover, the noncyclic, relatively flexible skeleton would allow it to form several stable coordination modes such that the intermediate species may become stable under the designated synthetic conditions.

RESULTS AND DISCUSSION

Preparation of the Tetradentate Chelate. The direct reaction of aniline with 2 equiv of protected 2-bromopyridine yields the appropriate dipyridylaniline, i.e., **L1**; see Scheme 1. This reaction is in contrast to certain C−N double-bond formation on functionalized aniline, for which isolation of the monopyridyl intermediate is recommended.[17] After that, hydrolysis of 1,3-dioxolane groups in **L1** afforded the acetyl compound **L2**, which could be converted to the bis(2-pyridylpyrazolate) chelate **L** by first Claisen condensation

Scheme 1. Synthetic Procedures to the Tetradentate Chelate L[a]

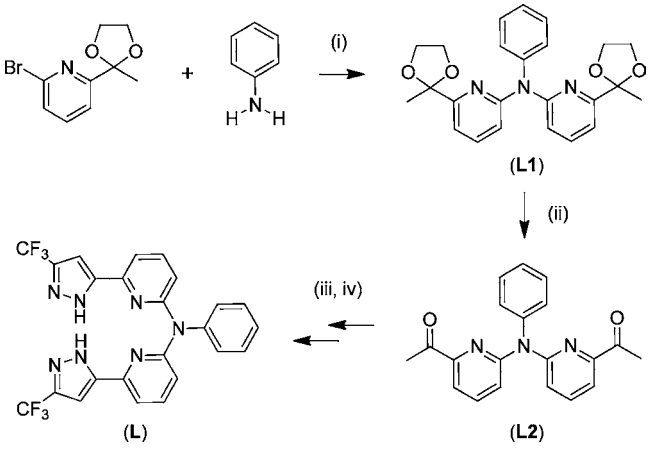

[a]Reagents and conditions: (i) $NaOBu^t$, $Pd_2(dba)_3$, DPPF, toluene, 100 °C, 24 h; (ii) 2 N HCl(aq), 80 °C, 12 h; (iii) CF_3CO_2Et, THF, 70 °C, 12 h; (iv) N_2H_4, ethanol, reflux, 36 h.

with ethyl trifluoroacetate, followed by cyclization employing hydrazine hydrate.

Preparation of Osmium(II) Complexes. It has been reported that $Os_3(CO)_{12}$ can react with 6 equiv of 3-(trifluoromethyl)-5-(2-pyridyl)pyrazole, the bidentate counterpart of the tetradentate chelate **L**, in refluxing diethylene glycol monomethyl ether (DGME) to afford the dicarbonyl complex $[Os(fppz)_2(CO)_2]$ (**1**),[18] for which the carbonyl ligands reside at the mutual cis orientation, while the pyrazolate and pyridyl substituents of fppz chelates are located at the trans and cis disposition, respectively. A structural drawing of **1** is depicted in Scheme 2. Furthermore, the treatment of **1** with freshly sublimed Me_3NO should kick off the coordinated carbonyls, followed by the addition of either PPh_2Me or $PPhMe_2$ to give $[Os(fppz)_2(PPh_2Me)_2]$ (**2**) and $[Os(fppz)_2(PPh_2Me_2)_2]$ (**3**) in high yields,[19] for which the fppz chelates turn to the planar and head-to-tail cyclic arrangements, with phosphines occupying the axial sites (Scheme 2).

With this precedence in mind, we then switched to the reaction of $Os_3(CO)_{12}$ with tetradentate **L** in an attempt to synthesize the respective $[Os(L)(CO)_2]$ (**4**). After routine chromophoric purification, it was then characterized by mass analysis, NMR spectroscopy, UV/vis, and emission spectral analyses. To our surprise, complex **4** showed no obvious emission in both solid and degassed solution at room temperature, which is in contrast to that of blue-emitting **1**, revealing the first indication of a difference in their bonding mode. A single-crystal X-ray diffraction study was next executed, for which the perspective view and selected bond lengths and angles are shown in Figure 1.

As can be seen, the tetradentate chelate **L** wraps around the Os^{II} metal center in a highly distorted manner, while the carbonyl groups take the mutual cis position with an angle of 89.55(16)°. Apparently, the competition for stronger dative bonding, i.e., the so-called trans effect, prevents these carbonyl groups from taking the mutual trans position.[20] Otherwise, the tetradentate chelate **L** would have adopted a planar geometry, which could have gained more stabilization than the present configuration. The Os−N distances of the **L** chelate vary considerably, for which the longest [Os−N(2) = 2.128(3) Å] and shortest [Os−N(6) = 2.044(3) Å] are due to the

dx.doi.org/10.1021/ic302829e | Inorg. Chem. 2013, 52, 5867−5875

Scheme 2. Structural Drawing of Osmium(II) Complexes with the Bidentate fppz Chelate

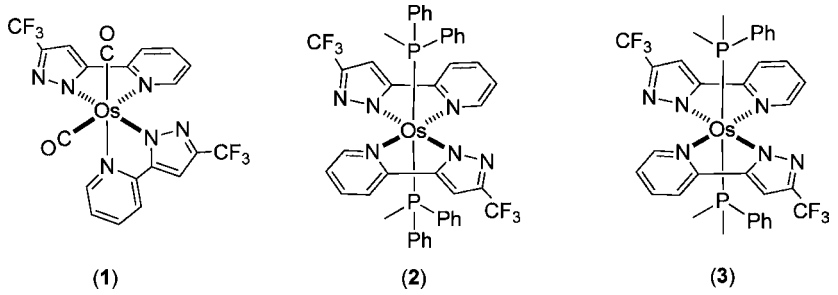

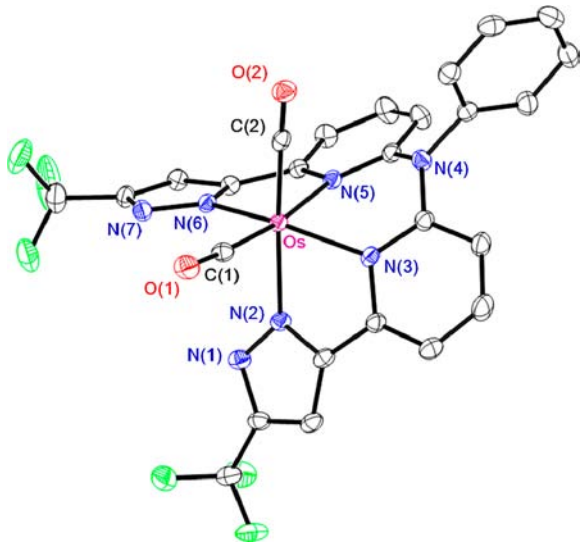

Figure 1. Perspective view of **4** with ellipsoids shown at the 40% probability level. Selected bond distances (Å) and angles (deg): Os–N(2) = 2.128(3), Os–N(3) = 2.090(3), Os–N(5) = 2.099(3), Os–N(6) = 2.044(3), Os–C(1) = 1.887(4), Os–C(2) = 1.888(4); C(1)–Os–C(2) = 89.55(16), C(1)–Os–N(5) = 172.76(15), N(3)–Os–N(5) = 81.57(13), C(2)–Os–N(2) = 170.73(14).

pyrazolates being trans to the carbonyl and pyridyl groups, respectively, and likewise can be attributed to the trans effect. Moreover, higher internal strain energy seems to be imposed at the central OsN(3)C(2) metallacycle, evidence of which are shown by the acute N(3)–Os–N(5) bond angle of 81.57(13)°, elongated Os–N(3) and Os–N(5) distances of 2.090(3) and 2.099(3) Å, respectively, and the adoption of a boatlike conformation rather than the planar geometry. Third, the arrangement of the four N-donor atoms of **4**, i.e., all cis arrangement for both the pyrazolate and pyridine groups, are analogous to that of neither its parent complex **1** nor the isomeric bis(pyridyltriazolate) complex $[Os(bptz)_2(CO)_2]$,[20] for which the anionic triazolate and neutral pyridyl fragments are located at the mutual cis and trans dispositions, respectively.

The phosphine-substituted complexes $[Os(L)(PPh_2Me)_2]$ (**5**) and $[Os(L)(PPhMe_2)_2]$ (**6**) were next prepared by the treatment of **4** with Me_3NO, followed by addition of the respective phosphines (Scheme 3). In an aim to simplify the synthetic procedure, we also made attempts to perform a one-pot method; i.e., after the reaction of $Os_3(CO)_{12}$ with **L**, we went directly to the Me_3NO and phosphine treatment and skipped isolation of the carbonyl intermediate **4**. This operation gave the anticipated complexes **5** and **6** in 22 and 29% yield, comparable to the total yields using the very complicated two-step process.

The structure of **5** is shown in Figure 2, with selected bond lengths and angles provided in the figure caption. The geometry of the Os^{II} center is a distorted octahedral, in which the diaxial positions are occupied by phosphines and the tetradentate chelate **L** takes the rest of the equatorial sites. In comparison, on the one hand, both of the Os–P distances [Os–P(1) = 2.3606(12) Å and Os–P(2) = 2.3648(12) Å] are comparable to those observed in parent complex **2** [2.3616(5) Å][19] and other osmium(II) complexes configured with trans-disposed phosphines.[11a] On the other hand, the Os–N distances seem to be notably different, i.e., the Os–N distances to ligated pyridyl groups [Os–N(3) = 2.044(4) Å and Os–N(5) = 2.037(4) Å], which turn out to be much shorter than the Os–N distances to the pyrazolates [Os–N(2) = 2.073(4) Å and Os–N(6) = 2.070(4) Å] at the peripheral, with the latter showing no variance to those in **2** [2.073(2) Å]. This reversal of the Os–N distances must be related to the formation of a central OsN(3)C(2) metallacycle, for which the phenylamido group forces the adjacent pyridyl groups to interact much tighter to the central Os^{II} atom. Moreover, the tetradentate chelate **L** adopts a slightly concave conformation, which is

Scheme 3. Transformation of Osmium(II) Complexes with the Tetradentate Chelate L[a]

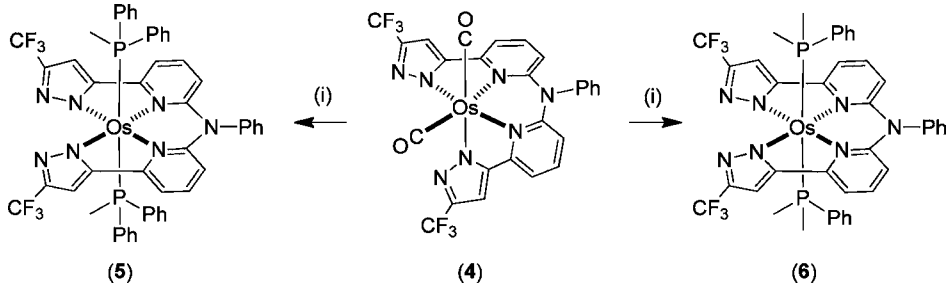

[a]Reagents and conditions: (i) Me_3NO, DGME, 120 °C, 1 h; $PPhMe_2$ (or PPh_2Me), 180 °C, 12 h.

dx.doi.org/10.1021/ic302829e | Inorg. Chem. 2013, 52, 5867–5875

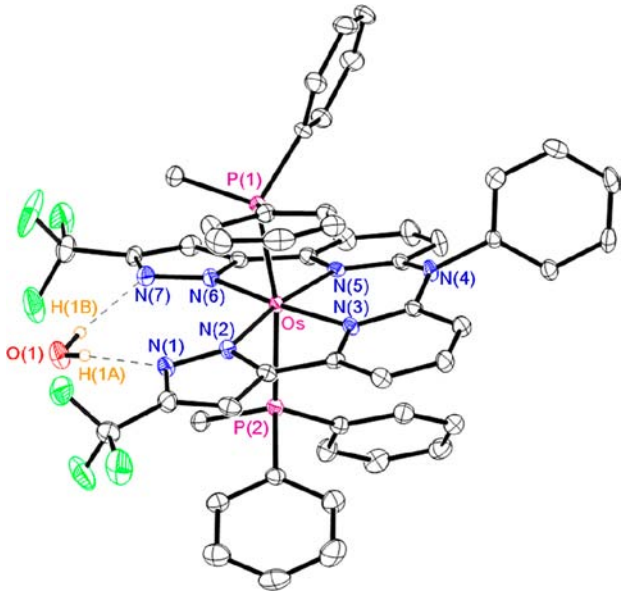

Figure 2. Perspective view of **5** with ellipsoids shown at the 40% probability level. Selected bond distances (Å) and angles (deg): Os–N(2) = 2.073(4), Os–N(3) = 2.044(4), Os–N(5) = 2.037(4), Os–N(6) = 2.070(4), Os–P(1) = 2.3606(12), Os–P(2) = 2.3648(12); P(1)–Os–P(2) = 169.61(4), N(2)–Os–N(6) = 109.49(15), N(3)–Os–N(5) = 93.68(15).

probably due to the packing effect within the crystal lattice. The uncoordinated N atom on both pyrazolates hydrogen-bonds with an adjacent solvated water, which is in sharp contrast to those in **2**; the latter showed the formation of an interligand hydrogen bond with the adjacent pyridyl group.[19]

Photophysics and Theoretical Work. The absorption and emission spectra of complexes **5** and **6** recorded in degassed CH_2Cl_2 at room temperature are displayed in Figure 3. For comparison, spectra of **2** and **3** are also depicted in Figure 3. All pertinent photophysical data of these complexes are summarized in Table 1. In general, complexes **5** and **6** exhibit allowed absorption bands in the UV region (<350 nm) and blue visible region (400–450 nm), for which ε values at the peak wavelengths around 335 and 420 nm are calculated to be ~3.5 × 10^4 and ~6.6 × 10^3 $M^{-1}\cdot cm^{-1}$, respectively, and can

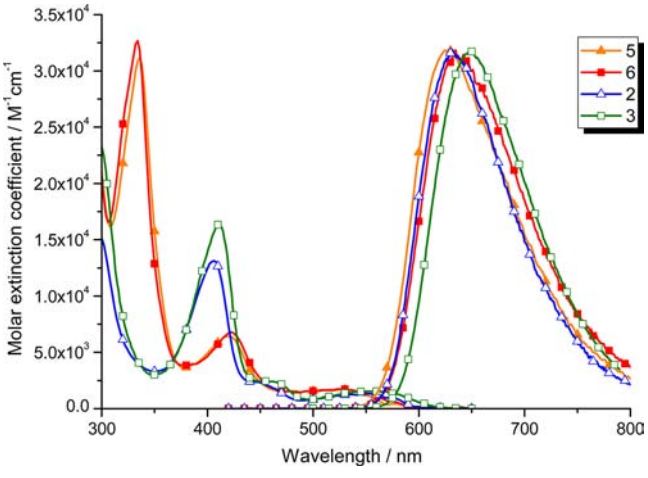

Figure 3. UV/vis absorption and emission spectra of osmium(II) complexes **2**, **3**, **5**, and **6** in a CH_2Cl_2 solution at room temperature.

thus be attributed to a ligand-centered (**L**; see Scheme 1) $\pi\pi^*$ transition. In comparison, these two $\pi\pi^*$ transition bands are obviously red-shifted with respect to the ~300 and 405 nm bands observed in **2** (or **3**), the result of which indicates the involvement of the bridging phenylamino group in the tetradentate chelate **L**, giving an elongation of π conjugation and, hence, a reduced ligand-centered $\pi\pi^*$ energy gap in the higher-lying electronic states for both complexes **5** and **6**.

The broad-band absorption at longer wavelength (>450 nm) for complexes **5** and **6** with relatively lower extinction coefficient (<3 × 10^3 $M^{-1}\cdot cm^{-1}$) is assigned to the metal d_π → pyridine (π^*) charge-transfer (MLCT), mixed to a certain extent with pyrazolate (π) → pyridine (π^*) intraligand charge transfer (ILCT) in the singlet manifold. This MLCT/ILCT band is about 22 nm (~760 cm^{-1}) blue-shifted with respect to that of the dual bidentate complexes **2** and **3**. From a chemistry point of view, the bridging phenylamido substituent in **5** and **6** acts as an electron-donating group, which is expected to raise the energy of the pyridine π^* orbital contributing to the lowest unoccupied molecular orbitals (LUMOs) of ILCT, resulting in an increase of the MLCT/ILCT band gap and hence a blue shift of the corresponding absorption peak wavelength.

Complexes **5** and **6** are highly emissive in both solution and the solid state, with the peak wavelengths appearing at 628 and 634 nm in degassed CH_2Cl_2 (see Figure 3). All emissions are confirmed as the phosphorescence because of their drastic quenching of the emission by O_2 upon aeration and relatively small radiative decay rate constant of k_r < 1 × 10^6 s^{-1}. Compared with **6**, the small blue shift of the emission in **5** may be rationalized by the slightly stronger electron-withdrawing PPh_2Me than that in **6**, resulting in a nonnegligible increase of the MLCT gap. For this case, the contribution of MLCT in the triplet manifold may accordingly be reduced in **5** (cf. **6**), as supported by the computational approach elaborated on in the following section. In comparison to the phosphorescence for **2** and **3**, shown in Figure 3, the hypsochromic shift of the emission for **5** and **6**, respectively, correlates well with the result of the blue shift of absorption for **5** and **6** (vide supra).

We then performed time-dependent density functional theory (TDDFT) calculations with the aim of gainig more insight into the fundamentals of the associated photophysical properties elaborated on above. Figure 4 presents the highest occupied molecular orbital (HOMO) and LUMO that are mostly involved in the lowest-lying transitions of **2** and **5** (see Figure S1 in the Supporting Information (SI) for more frontier orbitals of **2**, **3**, **5**, and **6**). It can be clearly seen from Figures 4 and S1 in the SI that, for complex **2** (also for **3**), the HOMO is predominantly located at the pyrazolate fragments and the central metal d_π orbitals, whereas the LUMO (and LUMO+1) shifts toward the pyridyl fragments. For complex **5** (also for **6**), because the two pyrazolate fragments are now trans to the two pyridyl fragments, the HOMO is contracted even more to the central metal d_π orbitals. As a result, the lowest-lying singlet and triplet transitions, which consist primarily of HOMO to LUMO or HOMO to LUMO+1 transitions, show a strong MLCT character for as high as 50–60% (see Table 2). Moreover, although of a very qualitative manner, the contribution of MLCT of 52% in the triplet states for **5** is slightly smaller than that of **6** (58%). This observation, in part, supports the aforementioned stronger electron-withdrawing properties of the ancillary PPh_2Me in **5** than in **6**.

The vertically excited energy states and their orbital decompositions based on the S_0-optimized geometries of **2**, **3**,

dx.doi.org/10.1021/ic302829e | Inorg. Chem. 2013, 52, 5867–5875

Table 1. Photophysical Data of Osmium(II) Complexes Measured in a Degassed CH_2Cl_2 Solution at Room Temperature and the Associated Electrochemical Properties

	abs λ_{max}/nm ($\varepsilon \times 10^{-3}$/M^{-1}·cm^{-1})	em λ_{max}/nm	Φ	τ_{obs}/ns	$k_r \times 10^{-5}$/s^{-1}	$k_{nr} \times 10^{-5}$/s^{-1}	$E_{1/2}^{ox}$/V [ΔE_p/mV[a]]	$E_{1/2}^{red}$/V [ΔE_p/mV[a]]
2	406 (16), 448 (2.4), 550 (1.3)	632	0.50	855	5.85	5.85	−0.10 [120]	−2.84 [100]
3	411 (21), 465 (2.4), 550 (1.5)	649	0.19	725	2.62	11.2	−0.17 [130]	−2.85 [130]
5	336 (31), 420 (6.4), 528 (1.7)	628	0.40	2070	1.94	2.89	−0.08 [90]	−2.82 [irr]
6	334 (33), 422 (6.8), 528 (1.7)	634	0.27	1690	1.62	4.32	−0.11 [90]	−2.80 [irr]

[a] $E_{1/2}$ (mV) refers to $[(E_{pa} + E_{pc})/2]$, where E_{pa} and E_{pc} are the anodic and cathodic peak potentials referenced to the Fc^+/Fc couple. $\Delta E_p = |E_{pa} - E_{pc}|$ was reported in millivolts, and the oxidation and reduction experiments were conducted in CH_2Cl_2 and THF solutions.

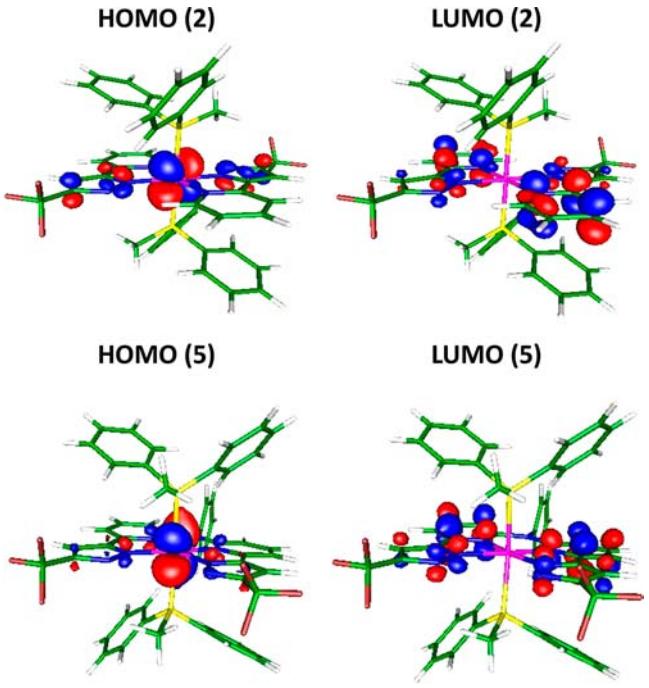

Figure 4. Electron density contours of the HOMO and LUMO for **2** and **5** based on the optimized ground state (S_0) geometries.

Table 2. Computational Energy Levels, Oscillator Strengths, and Orbital Transition Analyses of S_1 and T_1 States for Osmium(II) Complexes 2, 3, 5, and 6 Based on the Optimized S_0 Ground-State Geometries

compd	state	λ_{cal}/nm	f	assignment	MLCT/%
2	T_1	523	0	HOMO → LUMO (93%)	60
	S_1	498	0.005	HOMO → LUMO (98%)	61
3	T_1	543	0	HOMO → LUMO (94%)	60
	S_1	517	0.0032	HOMO → LUMO (98%)	61
5	T_1	514	0	HOMO → LUMO+1 (79%)	52
	T_2	512	0	HOMO → LUMO (82%)	
	S_1	467	0.0009	HOMO → LUMO (97%)	63
6	T_1	528	0	HOMO → LUMO (89%)	58
	T_2	516	0	HOMO → LUMO+1 (80%)	
	S_1	477	0.0004	HOMO → LUMO (97%)	61

5, and **6** are listed in Table 2. The calculated energy gaps of the S_0−S_1 transition for **2** (498 nm), **3** (517 nm), **5** (467 nm), and **6** (477 nm) reveal a trend similar to that observed experimentally, showing a lower-lying, broad absorption band peaked at 550 nm for **2** and **3** and 528 nm for **5** and **6** (see Table 1 and Figure 3). The discrepancy could be attributed to virtually the state mixing between singlet and triplet manifolds induced by the spin−orbit coupling. Such a coupling matrix should be substantial but is not considered in the current computational approach. The strong MLCT character of the S_0−S_1 transition corresponds well to the lower extinction coefficient observed in Figure 3. The increase of the energy gap due to the electron-donating phenylamido substituent in **5** and **6** is also reflected by the blue shift of the S_0−S_1 MLCT transition from **2** to **5** (or from **3** to **6**). For the emission properties, the calculated energy gaps of S_0−T_1 states using S_0 geometry for **2** (523 nm), **3** (543 nm), **5** (514 nm), and **6** (528 nm) are also in good agreement with the onset of the phosphorescence spectra.

To more accurately account for the emission spectra of these complexes, we made further attempts to locate the T_1 state by performing the geometry optimization along the triplet-state potential energy surface and then carefully examining the relative energy gaps between the ^{3}MLCT/$\pi\pi^*$ and triplet metal-centered (^{3}MC) dd states for the osmium(II) complexes **2**, **3**, **5**, and **6**. The ^{3}MC dd state involves d_{σ^*} antibonding and is considered to be the major nonradiative deactivation channel and the key factor in accounting for the instability.[1c] In this approach, on the one hand, the vertical energy gaps between the lowest triplet states, i.e., the ^{3}MLCT/$\pi\pi^*$ states, and S_0 match very well with the observed phosphorescence peaks for these complexes. On the other hand, the energy of the ^{3}MC dd state is located by a triplet geometry optimization starting from a distorted initial structure with highly lengthened metal−ligand bonds, as detailed in previous works.[20] For **2** and **3**, the ^{3}MC dd states are found to be 7.02 and 7.85 kcal·mol^{-1}, respectively, above the ^{3}MLCT/$\pi\pi^*$ states (see Figure S3 in the SI). As for the tetradentate complexes **5** and **6**, the energy of ^{3}MC dd states is even higher and cannot be stabilized by freely lengthening the metal−ligand bond due to the linkage of two pyridylpyrazolate moieties via the amido bridge. We thus conclude that the thermal population of the ^{3}MC dd state is even more unlikely for **5** and **6**; thus, the ^{3}MC dd state should not be an active channel for both nonradiative deactivation and photoinstability. This, together with the greater rigidity of terdentate moieties, accounts for the good phosphorescence yield for both **5** (0.40) and **6** (0.27) in a CH_2Cl_2 solution at room temperature and their suitability in the fabrication of OLEDs elaborated on below.

Electroluminescence of OLEDs. The as-prepared osmium(II) complexes are used as a red dopant in OLEDs. The devices are fabricated with the structure of ITO/NPB (60 nm)/TCTA (10 nm)/TPBi: metal complex (20 nm, 4 vol %)/TPBi (40 nm)/LiF(1 nm)/Al (150 nm). Device A contains the common red phosphorescent dopant tris(1-phenylisoquinoline)-C^2,*N*-iridium(III) [Ir(piq)$_3$], while devices B and C employ the newly prepared osmium(II) dopants **5** and **6**, respectively. In addition, 4,4′-bis[*N*-(1-naphthyl)-*N*-

dx.doi.org/10.1021/ic302829e | Inorg. Chem. 2013, 52, 5867−5875

phenylamino]biphenyl (NPB), 4,4′,4″-tris(*N*-carbazolyl)-triphenylamine (TCTA), and 1,3,5-tris(*N*-phenylbenzimidazol-2-yl)benzene (TPBi) function as a hole-transporting layer, an electron-blocking layer, and a host material or electron-transporting layer, respectively.

Figure 5 displays the EL spectra driven at the same current density of 5 mA·cm^{-2}. In principle, all three phosphors show

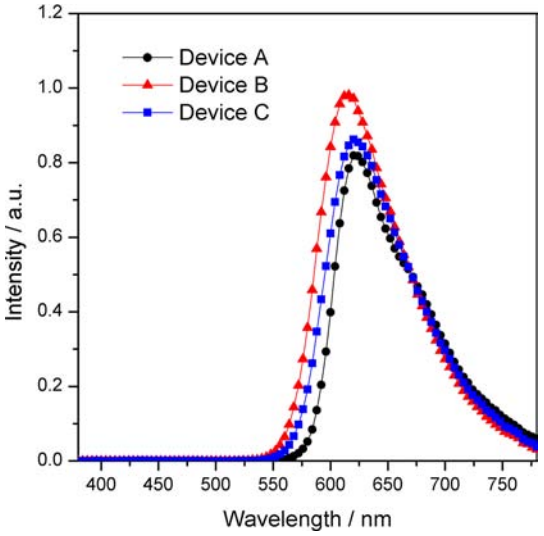

Figure 5. Respective EL spectra of devices A–C fabricated with emitter [Ir(piq)$_3$], **5**, and **6** at the same current density of 5 mA·cm^{-2}.

satisfactory deep-red emission with the CIE coordinates located at (0.67, 0.33), (0.63, 0.36), and (0.65, 0.35) for devices A–C, respectively. Concomitantly, osmium(II) phosphors **5** and **6** show structureless emission with centers located at 616 and 620 nm, which are in contrast with those of [Ir(piq)$_3$], showing an intense peak at 620 nm, together with a shoulder at 674 nm. Besides, complex **6** exhibits a much more red-shifted emission versus that of **5**, the result of which is consistent with the photoluminescence data shown in Figure 3 as well as the higher electron-donating nature of PPhMe$_2$ ancillaries.

Moreover, all of these devices exhibit good performance because of the effective exciton confinement and recombination in the emitting layer. As shown in Figure 6b,c, the devices with dopants **5** and **6** both exhibit EL properties superior to those of the reference device with [Ir(piq)$_3$]. The device with **5** shows the best performance characteristics with a maximum current efficiency of 14.0 cd·A^{-1} at 5 mA·cm^{-2} and an external quantum efficiency (EQE) of 9.8%; both are better than those for the reference device A with [Ir(piq)$_3$] showing a current efficiency of 7.6 cd·A^{-1} and an EQE of 8.5% at 10 mA·cm^{-2}. However, the osmium(II)-based devices B and C exhibit higher operation voltages than that of the [Ir(piq)$_3$] device, as shown in Figure 6a. This is caused by the shallow HOMO level of osmium(II) phosphors, which may induce a large carrier injection barrier and charge trap.[21] Devices B and C achieve maximum power efficiencies of 9.5 and 7.3 lm·W^{-1} (at 2.5 mA·cm^{-2}), respectively, while the reference device with [Ir(piq)$_3$] shows a slightly lower maximum power efficiency of 5.3 lm·W^{-1} (at 2.5 mA·cm^{-2}) under identical conditions. The combined device performance data are depicted in Table 3. It is believed that the power efficiency of devices B and C could be further improved if their drive voltage could be comparable to that of the reference device.

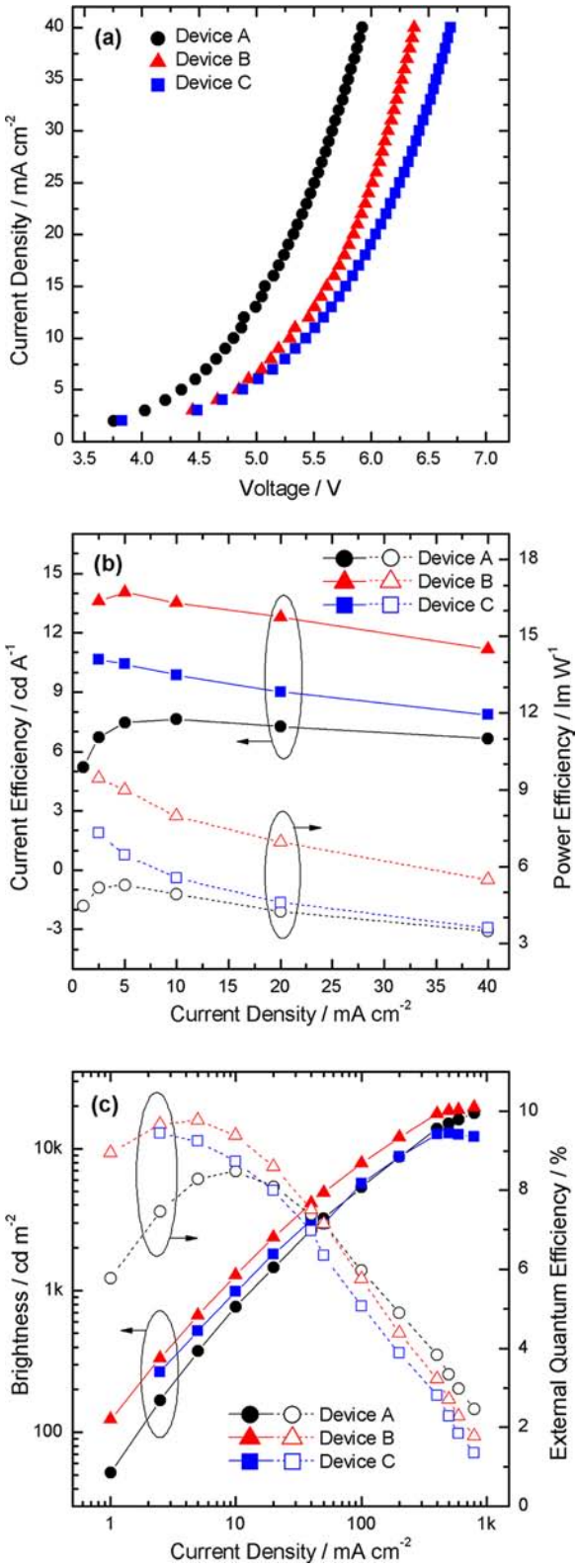

Figure 6. (a) Current density–voltage characteristics, (b) current efficiency–current density and power efficiency–current density relationships, and (c) brightness–current density and EQE–current density relationships for devices with different red dopants.

CONCLUSION

In summary, we have prepared the tetradentate bis-(pyridylpyrazolate) chelate **L** via the assembly of two bidentate

dx.doi.org/10.1021/ic302829e | *Inorg. Chem.* 2013, 52, 5867–5875

Table 3. EL Performances of Devices Fabricated with $[Ir(piq)_3]$, 5, and 6 as Phosphors

	dopant	V_{on}[b]/V	L_{max}/cd·m^{-2}	I_{max}/mA·cm^{-2}	$\eta_{ext,max}$/%	$\eta_{c,max}$/cd·A^{-1}	$\eta_{p,max}$/lm·W^{-1}	η_{ext}/%[c] at 1000 cd·m^{-2}	CIE [x, y]
A[a]	$[Ir(piq)_3]$	3.0	17800 (12.6 V)	800	8.5	7.6	5.3	5.1 (8.3 V)	0.67, 0.33
B[a]	**5**	3.3	19540 (11.6 V)	800	9.8	14.0	9.5	4.8 (9.5 V)	0.63, 0.36
C[a]	**6**	3.3	12900 (10.5 V)	500	9.4	10.6	7.3	5.6 (8.7 V)	0.65, 0.35

[a]The notations A–C indicate the devices fabricated with employment of dopants $[Ir(piq)_3]$, **5**, and **6**, respectively. [b]Turn-on voltage at which emission became detectable. [c]The driving voltage at 1000 cd·m^{-2} is depicted in parentheses.

3-(trifluoromethyl)-5-(2-pyridyl)pyrazole chelates at the 6 position of the pyridyl fragment with a phenylamido appendage. Subsequently, this chelate was utilized to prepare osmium(II) complexes **4**–**6**, among which the structures of **4** and **5** have been determined by single-crystal X-ray structural analysis. Phosphine-substituted derivatives **5** and **6** are highly emissive in both solution and the solid state. Thus, the OLED using dopant **5** exhibits a saturated red emission with a maximum brightness of 19540 cd·m^{-2} at 800 mA·cm^{-2} (11.6 V). The tetradentate coordination property is expected to offer an advantage in enhanced stability, and its extension in chemistry should be of great perspective because of the versatile derivation for the pyridylazolate moieties. This new progress should open up another dimension for the multidentate transition-metal complexes exploited in OLEDs and photovoltaics.

EXPERIMENTAL SECTION

General Procedures. All reactions were performed under nitrogen, and solvents were distilled from appropriate drying agents prior to use. Commercially available reagents were used without further purification unless otherwise stated. All reactions were monitored using precoated thin-layer chromatography plates (0.20 mm with fluorescent indicator UV254). 2-Bromo-6-(2-methyl-1,3-dioxolan-2-yl)pyridine was obtained by the treatment of 2-acetyl-6-bromopyridine with ethylene glycol in the presence of a catalytic amount of *p*-toluenesulfuric acid.[22] Mass spectra were obtained on a JEOL SX-102A instrument operating in electron impact or fast atom bombardment (FAB) mode. ^{1}H and ^{13}C NMR spectra were recorded on a Varian Mercury-400, an INOVA-500, or a Bruker AVANCE-600 instrument. Elemental analysis was carried out with a Heraeus CHN-O rapid elemental analyzer. Cyclic voltammetry measurements were performed using a BAS 100 B/W electrochemical analyzer. The oxidation and reduction measurements were recorded using a platinum wire and a gold disk coated with mercury as working electrodes, respectively, in anhydrous CH_2Cl_2 and anhydrous tetrahydrofuran (THF) containing 0.1 M $TBAPF_6$ as the supporting electrolyte, at a scan rate of 50 mV·s^{-1}. The potentials were measured against an Ag/Ag^+ (0.01 M $AgNO_3$) reference electrode with ferrocene as the internal standard.

Preparation of L1. A stirred solution of 2-bromo-6-(2-methyl-1,3-dioxolan-2-yl)pyridine (4.0 g, 16 mmol), aniline (0.70 g, 7.5 mmol), (1,1′-diphenylphosphino)ferrocene (DPPF; 0.33 g, 0.60 mmol), sodium *tert*-butoxide (2.0 g, 21 mmol), and $Pd_2(dba)_3$ (0.23 g, 0.25 mmol) in dried toluene (30 mL) was heated at 100 °C for 24 h. The reaction mixture was cooled to room temperature and neutralized with 2 N HCl(aq) until pH = 6–7. Extraction with CH_2Cl_2 (50 mL × 3) followed by evaporation of solvent produced the crude product, which was further purified by silica gel column chromatography, eluting with a 1:1 mixture of ethyl acetate and hexane. Yield: 2.7 g, 6.4 mmol, 87%.

Selected spectral data for **L1**. ^{1}H NMR (400 MHz, $CDCl_3$, 298 K): δ 7.51 (t, J_{HH} = 8.0 Hz, 2H), 7.35 (t, J_{HH} = 8.0 Hz, 2H), 7.21 (d, J_{HH} = 6.8 Hz, 3H), 7.10 (d, J_{HH} = 7.6 Hz, 2H), 6.95 (d, J_{HH} = 8.4 Hz, 2H), 4.00 (t, J_{HH} = 6.8 Hz, 4H), 3.87 (t, J_{HH} = 6.8 Hz, 4H), 1.59 (s, 6H).

Preparation of L2. To a 100 mL flask was added **L1** (2.7 g, 6.5 mmol) and 2 N HCl(aq) (30 mL). The solution was heated at 80 °C for 12 h. The mixture was cooled to room temperature and neutralized with 0.5 M NaOH(aq) until pH = 6–7. The product was then extracted with CH_2Cl_2 (30 mL × 3). The solution was concentrated, and the residue was separated by silica gel column chromatography, eluting with a 1:1 mixture of ethyl acetate and hexane. Recrystallization from mixed CH_2Cl_2 and hexane gave 2.0 g of yellow crystals (6.1 mmol, 94%).

Selected spectral data for **L2**. ^{1}H NMR (400 MHz, $CDCl_3$, 298 K): δ 7.70–7.64 (m, 4H), 7.44 (t, J_{HH} = 8.0 Hz, 2H), 7.33–7.26 (m, 5H), 2.38 (s, 6H).

Preparation of L. A mixture of **L2** (1.2 g, 3.5 mmol) and sodium ethoxide (0.68 g, 10 mmol) in 30 mL of THF was stirred at 0 °C for 1 h. After that, to the mixture was added ethyl trifluoroacetate (0.83 mL, 8.5 mmol), and it was heated at 70 °C for 12 h. After cooling to room temperature, the solvent was removed under reduced pressure and neutralized with 2 N HCl(aq) until pH = 4–5. Extraction with CH_2Cl_2 (50 mL × 3) followed by evaporation of solvent produced the crude diketone. Without further purification, this product was allowed to react with 98% hydrazine hydrate (3.4 mL, 70 mmol) in a refluxing ethanol solution for 36 h. After that, the solvent was removed under vacuum and the residue was washed with deionized water to remove the unreacted hydrazine. Further purification was carried out by silica gel column chromatography, eluting with a 1:1 mixture of ethyl acetate and hexane. Recrystallization from mixed ethyl acetate and hexane gave 1.2 g of a pale-yellow solid (2.3 mmol, 65%).

Selected spectral data for **L**. ^{1}H NMR (400 MHz, acetone-d_6, 298 K): δ 7.82 (t, J_{HH} = 8 Hz, 2H), 7.61 (d, J_{HH} = 7.6 Hz, 2H), 7.46 (t, J_{HH} = 8 Hz, 2H), 7.33–7.30 (m, 3H), 7.16 (s, 2H), 7.06 (d, J_{HH} = 8.4 Hz, 2H). ^{13}C NMR (150 MHz, $CDCl_3$, 298 K): δ 157.6 (s, 2C), 144.9 (s, 2C), 144.6 (s, 1C), 143.7 (q, J_{CF} = 38.3 Hz, 2C), 142.3 (s, 2C) 138.8 (s, 2C), 130.2 (s, 2C), 128.7 (s, 2C), 127.3 (s, 1C), 121.2 (q, J_{CF} = 268.7 Hz, 2C), 117.3 (s, 2C), 115.8 (s, 2C), 102.0 (s, 2C). ^{19}F NMR (376 MHz, $CDCl_3$, 298 K): δ −62.5 (s, 6F). Anal. Calcd for $C_{24}H_{15}F_6N_7$: C, 55.93; H, 2.93; N, 19.2. Found: C, 55.84; H, 3.03; N, 18.9.

Preparation of 4. To a 50 mL flask was added $Os_3(CO)_{12}$ (100 mg, 0.11 mmol), **L** (180 mg, 0.35 mmol), and DGME (20 mL). The mixture was heated at 190 °C for 24 h. After cooling to room temperature, the mixture was concentrated under reduced pressure and the resulting solid was washed with deionized water and diethyl ether. Further purification was carried out by silica gel column chromatography, eluting with a 3:1 mixture of ethyl acetate and hexane. Recrystallization from mixed ethyl acetate and hexane gave 95 mg of yellow crystals (**4**; 0.13 mmol, 38%). Single crystals suitable for X-ray diffraction were obtained from the slow diffusion of hexane into a CH_2Cl_2 solution saturated with the complex at room temperature.

Selected spectral data for **4**. ^{1}H NMR (400 MHz, acetone-d_6, 298 K): δ 8.07–8.00 (m, 2H), 7.92–7.89 (m, 3H), 7.83 (t, J_{HH} = 7.6 Hz, 2H), 7.74 (t, J_{HH} = 7.6 Hz, 1H), 7.67 (d, J_{HH} = 7.6 Hz, 1H), 7.27 (s, 1H), 7.18–7.09 (m, 3H). ^{19}F NMR (376 MHz, $CDCl_3$, 298K): δ −60.7 (s, 3F), −60.8 (s, 3F). Anal. Calcd for $C_{26}H_{13}F_6N_7O_2Os·H_2O$: C, 40.16; H, 1.94; N, 12.61. Found: C, 39.97; H, 2.09; N, 12.31.

Selected structural data of **4**: $C_{28.5}H_{19}F_6N_7O_2Os$, M = 795.71, monoclinic, space group $P2_1/n$, a = 13.0288(12) Å, b = 13.2670(13) Å, c = 16.9620(16) Å, β = 109.168(2)°, V = 2769.4(5) Å^3, Z = 4, ρ_{calcd} = 1.908 Mg·m^{-3}, $F(000)$ = 1540, crystal size = 0.40 × 0.15 × 0.06 mm^3, λ(Mo Kα) = 0.71073 Å, T = 150(2) K, μ = 4.687 mm^{-1}, 21102 reflections collected, 6339 independent reflections (R_{int} = 0.0442), GOF = 1.042, final R1 [$I > 2\sigma(I)$] = 0.0311, and wR2 (all data) = 0.0741.

Preparation of 5. To a 50 mL flask was added $Os_3(CO)_{12}$ (100 mg, 0.11 mmol), **L** (180 mg, 0.35 mmol), and DGME (20 mL). The

dx.doi.org/10.1021/ic302829e | Inorg. Chem. 2013, 52, 5867–5875

mixture was heated at 190 °C for 24 h. The solution was cooled to room temperature, trimethylamine *N*-oxide (52 mg, 0.66 mmol) was added, and the resulting mixture was briefly heated at 120 °C for 1 h. To this mixture was added PPh_2Me (0.14 mL, 0.73 mmol) at room temperature, and the mixture was then heated at 190 °C for 24 h. Finally, the solution was concentrated, and the residue was dissolved in ethyl acetate and washed with deionized water. Further purification was carried out by silica gel column chromatography, eluting with a 3:1 mixture of ethyl acetate and hexane. Recrystallization from mixed ethyl acetate and hexane gave red crystals of **5** (80 mg, 0.072 mmol, 22%). Single crystals of **5** were obtained by the slow diffusion of hexane into a CH_2Cl_2 solution saturated with the complex at room temperature. The derivative **6** was prepared using $PPhMe_2$ and under the similar procedure. Yield: 29%.

Selected spectral data for **5**. MS (FAB): m/z 1107 $[(M + 1)^+]$. ^{1}H NMR (400 MHz, acetone-d_6, 298 K): δ 7.80 (t, J_{HH} = 7.6 Hz, 2H), 7.71 (t, J_{HH} = 6.8 Hz, 1H), 7.35 (t, J_{HH} = 8.0 Hz, 2H), 7.19 (d, J_{HH} = 8.0 Hz, 2H), 7.13 (t, J_{HH} = 6.8 Hz, 6H), 6.99 (t, J_{HH} = 7.6 Hz, 8H), 6.87−6.86 (m, 8H), 6.73 (s, 2H), 5.88 (d, J_{HH} = 8.8 Hz, 2H), 1.04 (s, 6H). ^{13}C NMR (150 MHz, $CDCl_3$, 298 K): δ 156.8 (s, 1C), 151.5 (s, 2C), 148.3 (s, 2C), 143.3 (s, 2C), 142.8 (q, J_{CF} = 35.7 Hz, 2C), 131.6 (s, 2C), 130.8 (t, J_{CP} = 20.3 Hz, 4C), 130.4 (s, 8C), 130.2 (s, 2C), 129.8 (s, 1C), 129.5 (s, 2C), 128.6 (s, 4C), 127.8 (s, 8C), 122.3 (q, J_{CF} = 267.1 Hz, 2C), 113.0 (s, 2C), 112.0 (s, 2C), 102.0 (s, 2C), 9.9 (t, J_{CP} = 15.3 Hz, 2C). ^{19}F NMR (376 MHz, $CDCl_3$, 298 K): δ −59.8 (s, 6F). ^{31}P NMR (202 MHz, acetone-d_6, 298 K): δ −13.4 (s). Anal. Calcd for $C_{50}H_{39}F_6N_7OsP_2\cdot H_2O$: C, 53.52; H, 3.68; N, 8.74. Found: C, 53.11; H, 3.90; N, 8.80.

Selected structural data of **5**: $C_{50}H_{41}F_6N_7OOsP_2$, M = 1122.04, monoclinic, space group $P2_1/n$, a = 12.5123(9) Å, b = 20.0068(14) Å, c = 17.7109(12) Å, β = 93.438(2)°, V = 4425.6(5) Å^3, Z = 4, ρ_{calcd} = 1.684 Mg·m^{-3}, $F(000)$ = 2232, crystal size = 0.38 × 0.12 × 0.03 mm^3, λ(Mo Kα) = 0.71073 Å, T = 150(2) K, μ = 3.028 mm^{-1}, 27722 reflections collected, 10161 independent reflections (R_{int} = 0.0579), GOF = 1.081, final R1 $[I > 2\sigma(I)]$ = 0.0461, and wR2 (all data) = 0.0849.

Selected spectral data for **6**. MS (FAB): m/z 982 $[(M + 1)^+]$. ^{1}H NMR (400 MHz, acetone-d_6, 298 K): δ 7.74 (t, J_{HH} = 6.6 Hz, 2H), 7.65 (t, J_{HH} = 7.2 Hz, 1H), 7.45−7.37 (m, 4H), 7.14−7.10 (m, 4H), 6.95 (t, J_{HH} = 8 Hz, 6H), 6.30 (t, J_{HH} = 7.6 Hz, 4H), 5.70 (d, J_{HH} = 9.2 Hz, 2H), 0.76 (s, 12H). ^{13}C NMR (150 MHz, DMSO-d_6, 298 K): δ 155.6 (s, 1C), 150.6 (s, 2C), 147.2 (s, 2C), 142.7 (s, 2C), 141.3 (q, J_{CF} = 35.1 Hz, 2C), 133.2 (t, J_{CP} = 19.4 Hz, 2C), 131.0 (s, 4C), 129.7 (s, 4C), 129.6 (s, 2C), 128.9 (s, 1C), 127.6 (s, 2C), 127.4 (s, 2C), 126.6 (s, 2C), 122.5 (q, J_{CF} = 265.6 Hz, 2C), 112.7 (s, 2C), 111.4 (s, 2C), 101.3 (s, 2C), 7.4 (t, J_{CP} = 14.8 Hz, 2C). ^{19}F NMR (376 MHz, $CDCl_3$, 298 K): δ −59.7 (s, 6F). ^{31}P NMR (202 MHz, acetone-d_6, 298 K): δ −17.0 (s). Anal. Calcd for $C_{40}H_{35}F_6N_7OsP_2\cdot H_2O$: C, 47.29; H, 3.87; N, 9.65. Found: C, 46.96; H, 3.98; N, 9.45.

Single-Crystal X-ray Diffraction Studies. Single-crystal X-ray diffraction data were measured on a Bruker SMART Apex CCD diffractometer using Mo radiation (λ = 0.71073 Å). The data collection was executed using the *SMART* program. Cell refinement and data reduction were performed with the *SAINT* program. An empirical absorption was applied based on the symmetry-equivalent reflections and the *SADABS* program. The structures were solved using the *SHELXS-97* program and refined using the *SHELXL-97* program by full-matrix least squares on F^2 values. The structural analysis and molecular graphics were obtained using the *SHELXTL* program on a PC computer.[23]

Photophysical Measurement. Measurement of the steady-state absorption, emission, and phosphorescence lifetimes in both solution and the solid state was described in our previous reports.[24] To determine the phosphorescence quantum yield (QY) in solution, the samples were degassed by three freeze−pump−thaw cycles. A fluorescence dye, 4-(dicyanomethylene)-2-methyl-6-(4-dimethylaminostyryl)-4*H*-pyran (λ_{max} = 615 nm; QY = 0.44 in methanol), was used as the standard reference for the QY measurement. Lifetime studies were measured with an Edinburgh FL 900 photon-counting system and a hydrogen lamp as the excitation source. Data were fitted by the sum of the exponential functions with a temporal resolution of ∼300 ps by using a nonlinear least-squares procedure in combination with an iterative convolution method.

Computational Methodology. Calculations on the electronic singlet and triplet states of all titled complexes were carried out using the DFT with B3LYP hybrid functional.[25] Restricted and unrestricted formalisms were adopted in the singlet and triplet geometry optimization, respectively. A "double-ζ" quality basis set consisting of Hay and Wadt's effective core potentials (ECPs; LANL2DZ)[26] was employed for the Ir^{III} metal atom, and a 6-31G* basis set,[27] for the rest of the atoms. The relativistic ECPs replaced the inner-core electrons of the Os^{II} metal atom, leaving only the outer-core valence electrons ($5s^25p^65d^6$) to be concerned with. TDDFT calculations using the B3LYP functional were then performed based on the optimized structures at ground states.[28] Moreover, considering the solvation effect, the calculations were then combined with an integral equation formalism polarizable continuum model (IEF-PCM in dichloromethane), implemented in *Gaussian 09*.[29] Typically, 10 lower triplet and singlet roots of the nonhermitian eigenvalue equations were obtained to determine the vertical excitation energies. The oscillator strengths were then deduced from dipole transition matrix elements (for singlet states only). All calculations were carried out using *Gaussian 09*.[30]

Fabrication and Characterization of OLEDs. The OLEDs are fabricated on prepatterned indium−tin oxide (ITO) substrates with a sheet resistance of 10 Ω·square^{-1} and an optical transmittance over 85% in the visible spectral range. Before being used, the ITO substrates are cleaned in an ultrasonic bath of acetone, alcohol, and deionized water, respectively, and treated by UV ozone for 15 min to enhance the work function of the ITO anode. All materials are deposited on the ITO substrates in a vacuum thermal evaporator without breaking the vacuum. All of the devices are encapsulated in a nitrogen-filled glovebox after being removed from the evaporator. The fabricated devices are then characterized at room temperature in air. The electrical and EL properties of the devices are measured with a constant-current source meter (Keithley 2400) and photometer (Photoresearch PR-650).

■ ASSOCIATED CONTENT

Supporting Information

X-ray crystallographic data file (CIF) of **4** and **5** and detailed results concerning the TDDFT calculations of all studied osmium(II) complexes. This material is available free of charge via the Internet at http://pubs.acs.org.

■ AUTHOR INFORMATION

Corresponding Author

*E-mail: ychi@mx.nthu.edu.tw (Y.C.), lsliao@suda.edu.cn (L.-S.L.), eliseytli@ntnu.edu.tw (E.Y.L.).

Notes

The authors declare no competing financial interest.

■ ACKNOWLEDGMENTS

This work was supported by the Cross-Strait Collaboration Fund sponsored by both the National Science Council (Grant 100-2119-M-001-030-MY3) and the National Natural Science Foundation of China (Grant 21161160446).

■ REFERENCES

(1) (a) Sasabe, H.; Kido, J. *Chem. Mater.* **2011**, *23*, 621. (b) Duan, L.; Hou, L.; Lee, T.-W.; Qiao, J.; Zhang, D.; Dong, G.; Wang, L.; Qiu, Y. *J. Mater. Chem.* **2010**, *20*, 6392. (c) Chi, Y.; Chou, P.-T. *Chem. Soc. Rev.* **2010**, *39*, 638. (d) Zhou, G.; Wong, W.-Y.; Suo, S. *J. Photochem. Photobiol. C* **2010**, *11*, 133. (e) You, Y.; Park, S. Y. *Dalton Trans.* **2009**, 1267. (f) Wong, W.-Y.; Ho, C.-L. *Coord. Chem. Rev.* **2009**, *253*, 1709. (g) Ulbricht, C.; Beyer, B.; Friebe, C.; Winter, A.; Schubert, U. S. *Adv. Mater.* **2009**, *21*, 4418. (h) Wong, W.-Y.; Ho, C.-L. *J. Mater. Chem.*

2009, *19*, 4457. (i) Williams, J. A. G.; Wilkinson, A. J.; Whittle, V. L. *Dalton Trans.* **2008**, 2081.
(2) (a) Hwang, F.-M.; Chen, H.-Y.; Chen, P.-S.; Liu, C.-S.; Chi, Y.; Shu, C.-F.; Wu, F.-I.; Chou, P.-T.; Peng, S.-M.; Lee, G.-H. *Inorg. Chem.* **2005**, *44*, 1344. (b) Nazeeruddin, M. K.; Gratzel, M. *Struct. Bonding (Berlin)* **2007**, *123*, 113. (c) Zhou, G.; Ho, C.-L.; Wong, W.-Y.; Wang, Q.; Ma, D.; Wang, L.; Lin, Z.; Marder, T. B.; Beeby, A. *Adv. Funct. Mater.* **2008**, *18*, 499. (d) Zhou, G.-J.; Wang, Q.; Wong, W.-Y.; Ma, D.; Wang, L.; Lin, Z. *J. Mater. Chem.* **2009**, *19*, 1872. (e) Ho, C.-L.; Wang, Q.; Lam, C.-S.; Wong, W.-Y.; Ma, D.; Wang, L.; Gao, Z.-Q.; Chen, C.-H.; Cheah, K.-W.; Lin, Z. *Chem.—Asian J.* **2009**, *4*, 89. (f) Zhou, G.; Wang, Q.; Wang, X.; Ho, C.-L.; Wong, W.-Y.; Ma, D.; Wang, L.; Lin, Z. *J. Mater. Chem.* **2010**, *20*, 7472. (g) Zhou, G.; Wong, W.-Y.; Yang, X. *Chem.—Asian J.* **2011**, *6*, 1706. (h) Ho, C.-L.; Chi, L.-C.; Hung, W.-Y.; Chen, W.-J.; Lin, Y.-C.; Wu, H.; Mondal, E.; Zhou, G.-J.; Wong, K.-T.; Wong, W.-Y. *J. Mater. Chem.* **2012**, *22*, 215.
(3) (a) Kober, E. M.; Sullivan, B. P.; Meyer, T. J. *Inorg. Chem.* **1984**, *23*, 2098. (b) Yersin, H.; Humbs, W.; Strasser, J. *Coord. Chem. Rev.* **1997**, *159*, 325. (c) Carlson, B.; Phelan, G. D.; Benedict, J.; Kaminsky, W.; Dalton, L. *Inorg. Chim. Acta* **2004**, *357*, 3967. (d) Carlson, B.; Phelan, G. D.; Kaminsky, W.; Dalton, L.; Jiang, X. Z.; Liu, S.; Jen, A. K.-Y. *J. Am. Chem. Soc.* **2002**, *124*, 14162.
(4) (a) Bernhard, S.; Gao, X.; Malliaras, G. G.; Abruna, H. D. *Adv. Mater.* **2002**, *14*, 433. (b) Hosseini, A. R.; Koh, C. Y.; Slinker, J. D.; Flores-Torres, S.; Abruna, H. D.; Malliaras, G. G. *Chem. Mater.* **2005**, *17*, 6114.
(5) Kober, E. M.; Marshall, J. L.; Dressick, W. J.; Sullivan, B. P.; Caspar, J. V.; Meyer, T. J. *Inorg. Chem.* **1985**, *24*, 2755.
(6) (a) Chen, Y.-L.; Lee, S.-W.; Chi, Y.; Hwang, K.-C.; Kumar, S. B.; Hu, Y.-H.; Cheng, Y.-M.; Chou, P.-T.; Peng, S.-M.; Lee, G.-H.; Yeh, S.-J.; Chen, C.-T. *Inorg. Chem.* **2005**, *44*, 4287. (b) Chung, L.-H.; Chan, S.-C.; Lee, W.-C.; Wong, C.-Y. *Inorg. Chem.* **2012**, *51*, 8693.
(7) Hwang, K.-C.; Chen, J.-L.; Chi, Y.; Lin, C.-W.; Cheng, Y.-M.; Lee, G.-H.; Chou, P.-T.; Lin, S.-Y.; Shu, C.-F. *Inorg. Chem.* **2008**, *47*, 3307.
(8) Tung, Y.-L.; Lee, S.-W.; Chi, Y.; Tao, Y.-T.; Chien, C.-H.; Cheng, Y.-M.; Chou, P.-T.; Peng, S.-M.; Liu, C.-S. *J. Mater. Chem.* **2005**, *15*, 460.
(9) Cheng, Y.-M.; Li, E. Y.; Lee, G.-H.; Chou, P.-T.; Lin, S.-Y.; Shu, C.-F.; Hwang, K.-C.; Chen, Y.-L.; Song, Y.-H.; Chi, Y. *Inorg. Chem.* **2007**, *46*, 10276.
(10) (a) Hsu, F.-C.; Tung, Y.-L.; Chi, Y.; Hsu, C.-C.; Cheng, Y.-M.; Ho, M.-L.; Chou, P.-T.; Peng, S.-M.; Carty, A. J. *Inorg. Chem.* **2006**, *45*, 10188. (b) Du, B.-S.; Liao, J.-L.; Huang, M.-H.; Lin, C.-H.; Lin, H.-W.; Chi, Y.; Pan, H.-A.; Fan, G.-L.; Wong, K.-T.; Lee, G.-H.; Chou, P.-T. *Adv. Funct. Mater.* **2012**, *22*, 3491.
(11) (a) Lee, T.-C.; Hung, J.-Y.; Chi, Y.; Cheng, Y.-M.; Lee, G.-H.; Chou, P.-T.; Chen, C.-C.; Chang, C.-H.; Wu, C.-C. *Adv. Funct. Mater.* **2009**, *19*, 2639. (b) Chen, J.-L.; Chi, Y.; Chen, K.; Cheng, Y.-M.; Chung, M.-W.; Yu, Y.-C.; Lee, G.-H.; Chou, P.-T.; Shu, C.-F. *Inorg. Chem.* **2010**, *49*, 823.
(12) (a) Che, C.-M.; Chan, S.-C.; Xiang, H.-F.; Chan, M. C. W.; Liu, Y.; Wang, Y. *Chem. Commun.* **2004**, 1484. (b) Castellano, F. N.; Pomestchenko, I. E.; Shikhova, E.; Hua, F.; Muro, M. L.; Rajapakse, N. *Coord. Chem. Rev.* **2006**, *250*, 1819. (c) Williams, J. A. G.; Develay, S.; Rochester, D. L.; Murphy, L. *Coord. Chem. Rev.* **2008**, *252*, 2596. (d) Zhao, Q.; Li, F.; Huang, C. *Chem. Soc. Rev.* **2010**, *39*, 3007. (e) Kalinowski, J.; Fattori, V.; Cocchi, M.; Williams, J. A. G. *Coord. Chem. Rev.* **2011**, *255*, 2401. (f) Wong, K. M.-C.; Yam, V. W.-W. *Acc. Chem. Res.* **2011**, *44*, 424. (g) Li, K.; Guan, X.; Ma, C.-W.; Lu, W.; Chen, Y.; Che, C.-M. *Chem. Commun.* **2011**, *47*, 9075.
(13) (a) Sauvage, J. P.; Collin, J. P.; Chambron, J. C.; Guillerez, S.; Coudret, C.; Balzani, V.; Barigelletti, F.; De Cola, L.; Flamigni, L. *Chem. Rev.* **1994**, *94*, 993. (b) Meyer, T. J.; Huynh, M. H. V. *Inorg. Chem.* **2003**, *42*, 8140. (c) Benniston, A. C.; Harriman, A.; Li, P.; Sams, C. A. *J. Phys. Chem. A* **2005**, *109*, 2302.
(14) (a) Halcrow, M. A. *Coord. Chem. Rev.* **2005**, *249*, 2880. (b) Schulze, B.; Friebe, C.; Hager, M. D.; Winter, A.; Hoogenboom, R.; Goerls, H.; Schubert, U. S. *Dalton Trans.* **2009**, 787. (c) Williams, J. A. G. *Chem. Soc. Rev.* **2009**, *38*, 1783.
(15) (a) Gentemann, S.; Albaneze, J.; Garcia-Ferrer, R.; Knapp, S.; Potenza, J. A.; Schugar, H. J.; Holten, D. *J. Am. Chem. Soc.* **1994**, *116*, 281. (b) Cheng, W. K.; Wong, K. Y.; Tong, W. F.; Lai, T. F.; Che, C. M. *J. Chem. Soc., Dalton Trans.* **1992**, 91.
(16) Chou, P.-T.; Chi, Y. *Chem.—Eur. J.* **2007**, *13*, 380.
(17) Allen, J. J.; Hamilton, C. E.; Barron, A. R. *Dalton Trans.* **2010**, *39*, 11451.
(18) Wu, P.-C.; Yu, J.-K.; Song, Y.-H.; Chi, Y.; Chou, P.-T.; Peng, S.-M.; Lee, G.-H. *Organometallics* **2003**, *22*, 4938.
(19) Tung, Y.-L.; Wu, P.-C.; Liu, C.-S.; Chi, Y.; Yu, J.-K.; Hu, Y.-H.; Chou, P.-T.; Peng, S.-M.; Lee, G.-H.; Tao, Y.; Carty, A. J.; Shu, C.-F.; Wu, F.-I. *Organometallics* **2004**, *23*, 3745.
(20) Yu, J.-K.; Hu, Y.-H.; Cheng, Y.-M.; Chou, P.-T.; Peng, S.-M.; Lee, G.-H.; Carty, A. J.; Tung, Y.-L.; Lee, S.-W.; Chi, Y.; Liu, C.-S. *Chem.—Eur. J.* **2004**, *10*, 6255.
(21) (a) Wu, F.-I.; Shih, P.-I.; Shu, C.-F.; Tung, Y.-L.; Chi, Y. *Macromolecules* **2005**, *38*, 9028. (b) Niu, Y.-H.; Tung, Y.-L.; Chi, Y.; Shu, C.-F.; Kim, J. H.; Chen, B.; Luo, J.; Carty, A. J.; Jen, A. K.-Y. *Chem. Mater.* **2005**, *17*, 3532.
(22) Chen, K.-S.; Liu, W.-H.; Wang, Y.-H.; Lai, C.-H.; Chou, P.-T.; Lee, G.-H.; Chen, K.; Chen, H.-Y.; Chi, Y.; Tung, F.-C. *Adv. Funct. Mater.* **2007**, *17*, 2964.
(23) Sheldrick, G. M. *Acta Crystallogr.* **2008**, *A64*, 112.
(24) Chou, P.-T.; Yu, W.-S.; Cheng, Y.-M.; Pu, S.-C.; Yu, Y.-C.; Lin, Y.-C.; Huang, C.-H.; Chen, C.-T. *J. Phys. Chem. A* **2004**, *108*, 6487.
(25) (a) Lee, C.; Yang, W.; Parr, R. G. *Phys. Rev. B* **1988**, *37*, 785. (b) Becke, A. D. *J. Chem. Phys.* **1993**, *98*, 5648.
(26) (a) Hay, P. J.; Wadt, W. R. *J. Chem. Phys.* **1985**, *82*, 299. (b) Hay, P. J.; Wadt, W. R. *J. Chem. Phys.* **1985**, *82*, 284.
(27) Hariharan, P. C.; Pople, J. A. *Mol. Phys.* **1974**, *27*, 209.
(28) (a) Jamorski, C.; Casida, M. E.; Salahub, D. R. *J. Chem. Phys.* **1996**, *104*, 5134. (b) Petersilka, M.; Gossmann, U. J.; Gross, E. K. U. *Phys. Rev. Lett.* **1996**, *76*, 1212. (c) Bauernschmitt, R.; Ahlrichs, R.; Hennrich, F. H.; Kappes, M. M. *J. Am. Chem. Soc.* **1998**, *120*, 5052. (d) Casida, M. E.; Jamorski, C.; Casida, K. C.; Salahub, D. R. *J. Chem. Phys.* **1998**, *108*, 4439. (e) Stratmann, R. E.; Scuseria, G. E.; Frisch, M. J. *J. Chem. Phys.* **1998**, *109*, 8218.
(29) Cancès, E.; Mennucci, B.; Tomasi, J. *J. Chem. Phys.* **1997**, *107*, 3032.
(30) Frisch, M. J.; Trucks, G. W.; Schlegel, H. B.; Scuseria, G. E.; Robb, M. A.; Cheeseman, J. R.; Scalmani, G.; Barone, V.; Mennucci, B.; Petersson, G. A.; Nakatsuji, H.; Caricato, M.; Li, X.; Hratchian, H. P.; Izmaylov, A. F.; Bloino, J.; Zheng, G.; Sonnenberg, J. L.; Hada, M.; Ehara, M.; Toyota, K.; Fukuda, R.; Hasegawa, J.; Ishida, M.; Nakajima, T.; Honda, Y.; Kitao, O.; Nakai, H.; Vreven, T.; Montgomery, J. A.; Peralta, J. E.; Ogliaro, F.; Bearpark, M.; Heyd, J. J.; Brothers, E.; Kudin, K. N.; Staroverov, V. N.; Kobayashi, R.; Normand, J.; Raghavachari, K.; Rendell, A.; Burant, J. C.; Iyengar, S. S.; Tomasi, J.; Cossi, M.; Rega, N.; Millam, J. M.; Klene, M.; Knox, J. E.; Cross, J. B.; Bakken, V.; Adamo, C.; Jaramillo, J.; Gomperts, R.; Stratmann, R. E.; Yazyev, O.; Austin, A. J.; Cammi, R.; Pomelli, C.; Ochterski, J. W.; Martin, R. L.; Morokuma, K.; Zakrzewski, V. G.; Voth, G. A.; Salvador, P.; Dannenberg, J. J.; Dapprich, S.; Daniels, A. D.; Farkas; Foresman, J. B.; Ortiz, J. V.; Cioslowski, J.; Fox, D. J. *Gaussian 09* revision A.1; Gaussian Inc.: Wallingford, CT, 2009.